Automatic Classification of Cochlear Implant Electrode Cavity Positioning

Jack H. Noble[1,2(✉)], Robert F. Labadie[2], and Benoit M. Dawant[1]

[1] Department of Electrical Engineering and Computer Science, Vanderbilt University, Nashville, TN 37235, USA
jack.noble@vanderbilt.edu
[2] Department of Otolaryngology – Head and Neck Surgery, Vanderbilt University Medical Center, Nashville, TN 37232, USA

Abstract. Cochlear Implants (CIs) restore hearing using an electrode array that is surgically implanted into the intra-cochlear cavities. Research has indicated that each electrode can lie in one of several cavities and that location is significantly associated with hearing outcomes. However, comprehensive analysis of this phenomenon has not been possible because the cavities are not directly visible in clinical CT images and because existing methods to estimate cavity location are not accurate enough, labor intensive, or their accuracy has not been validated. In this work, a novel graph-based search is presented to automatically identify the cavity in which each electrode is located. We test our approach on CT scans from a set of 34 implanted temporal bone specimens. High resolution μCT scans of the specimens, where cavities are visible, show our method to have 98% cavity classification accuracy. These results indicate that our methods could be used on a large scale to study the link between electrode placement and outcome, which could lead to advances that improve hearing outcomes for CI users.

Keywords: Cochlear implant · Graph search · Scalar location

1 Introduction

Cochlear implants (CIs) are considered the standard of care treatment for profound hearing loss [1]. CIs use an array of electrodes surgically implanted into the cochlea (see Fig. 1) to directly stimulate the auditory nerve, inducing the sensation of hearing. Although CIs have been remarkably successful, speech recognition ability remains highly variable across CI recipients. Research has indicated that each electrode can lie in one of several intra-cochlear cavities and that array cavity location is significantly associated with hearing outcomes [2–6]. However, comprehensive analysis of this phenomenon has not been possible because the cavity position for each individual electrode has been unknown. Electrode position is generally unknown in surgery because the array is blindly threaded into a small opening of the cochlea. To analyze the relationship between electrode position and outcome, several groups have proposed post-operative imaging techniques. But these processes have been relatively imprecise because visual assessment in CT images can only indicate coarse array positioning,

A. F. Frangi et al. (Eds.): MICCAI 2018, LNCS 11073, pp. 47–54, 2018.
https://doi.org/10.1007/978-3-030-00937-3_6

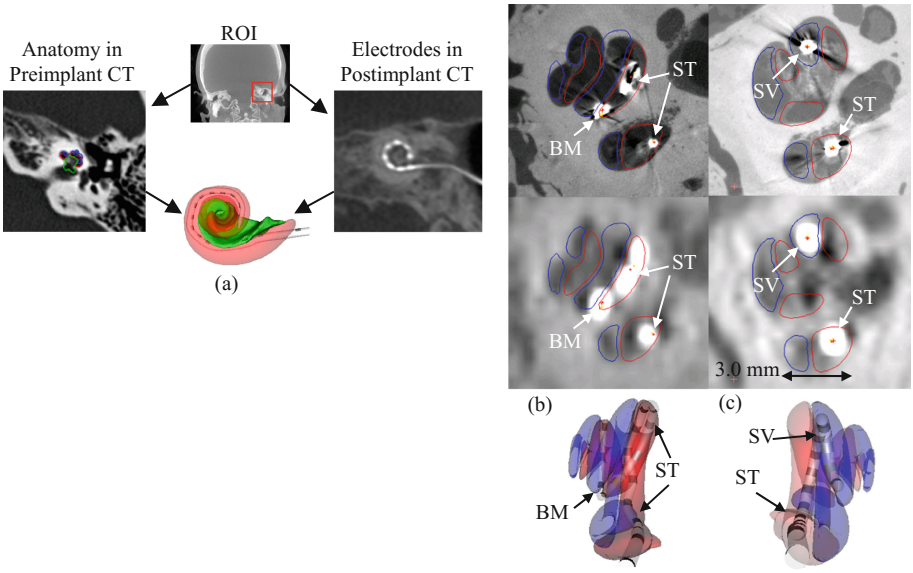

Fig. 1. (a) Pre-processing flow chart. The position of the electrodes relative to intracochlear anatomy (ST = red, modiolus = green) is found by registering preimplant CT anatomy segmentations to postimplant CT electrode localizations. In (b) and (c) different electrode position classifications for two cases are shown in μCT (top row) and CT (middle row) overlaid with automatic, CT-based anatomy localizations (ST = red, SV = blue). The bottom row shows automatic anatomy and electrode localizations in 3D.

e.g., whether or not the array is entirely within one internal cavity of the cochlea, rather than specifying cavity location for each individual electrode. Thus, studies have concluded that electrode position and outcomes are correlated but conclusions are vague and conflict across studies regarding precise relationships, such as the relationship between outcomes and the number of electrodes that lie in each cavity. Dataset size has also been limited in many studies, in part due to the amount of manual effort that must be undertaken to analyze the images when automatic techniques are not available. In the current work, we propose a fully automatic approach for localizing the cavity position of individual CI electrodes. Such an approach could permit analysis on large numbers of datasets to better study the relationship between electrode position and outcome, which may lead to advances in implant design or surgical techniques.

To determine the cavity in which each electrode is located, we start with an accurate but imperfect localization of the centroid of each electrode and segmentations of the principal intra-cochlear cavities, the scala tympani (ST) and scala vestibuli (SV) (see Fig. 1). The electrodes are automatically localized in postimplantation CT [7, 8], where the electrode array can be well visualized; the intra-cochlear cavities are automatically localized in preimplantation CT [9], where there are no implant related artifacts present and the cochlea can be visualized; and the two results are registered as shown in Fig. 1a. While the external walls of the cochlea are visible in CT, the borders between the intra-cochlear cavities are not directly visible due to the micron scale of the

structures separating the cavities as shown in Fig. 1b. Thus, we use a technique where the external walls of the cochlea are used as landmarks to estimate the invisible borders of the intracochlear cavities. To do this, a statistical shape model was constructed using high resolution μCT imaging of cochleae specimens where intracochlear borders are visible. μCT can be acquired for specimens but not *in vivo* due to radiation and size considerations. The external wall portion of the model is fitted to the walls of the cochlea visible in the patient CT image, and the model statistically estimates the shape and position of the intracochlear cavities based on the wall shape.

It is possible to directly estimate the cavity location of each electrode using these data. However, while these techniques to localize the cavities and the electrodes have been shown to be accurate, they are prone to small errors, and small localization errors can result in cavity classification errors. In this work, we present the first validation study on the use of these image processing techniques for electrode cavity classification. As our results will show, classification of the cavity position of each electrode using these data can be done more accurately by using a method that is robust to errors in the localization results. We present a novel graph search-based algorithm that is robust to localization errors to classify the cavity position of each contact. We validate our approach with a set of 34 cochlea specimens. For each specimen, we run our automatic algorithm on pre- and postimplantation CTs. We compute the accuracy of our results by comparing them to the ground truth cavity location, which is defined using high resolution μCT imaging.

2 Methods

To more robustly estimate the cavity position of each electrode compared to direct estimation based on the image processing results, we assume that the classification of neighboring electrodes on the array should be relatively consistent. In other words, if both flanking electrodes in a group of three lie within and distant to the border of the scala tympani, it is highly likely that the central electrode also lies in the scala tympani. To implement a search that exploits this heuristic, we develop a graph search-based classification solution that permits defining penalties for class transitions between electrodes and finding a solution that globally optimizes our classification criteria. The graph $G = \{V, E\}$ we have designed is shown in Fig. 2. This is a directed-acyclic graph where the N middle columns of nodes correspond to the N electrodes in the array, and the three rows of the N middle columns correspond to the three possible cavity classifications for each electrode (ST = scala tympani, SV = scala vestibuli, and BM = basilar membrane). The ST and SV classifications correspond to electrodes that fall within the scala tympani or scala vestibuli. The BM classification corresponds to electrodes that have violated the basilar membrane that separates the ST and SV and sit between the ST and SV in the region where the BM was located preimplantation. Electrodes belonging to these three classifications are shown in CT and μCT and in 3D in Fig. 1b.

The graph is designed such that a path from the seed to the endnode will include one and only one of the three nodes that belong to each of the N electrodes. Thus, with this graph, a path that connects the seed to the endnode also implies a cavity

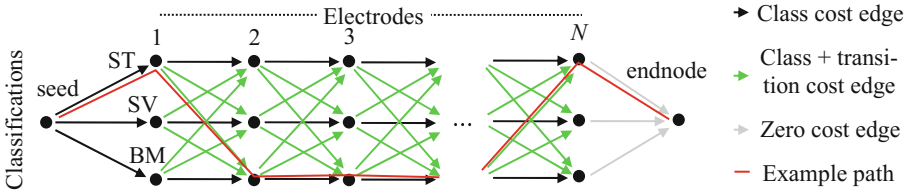

Fig. 2. Graph (black, green, and gray) that is used to classify the cavity location of each of the N electrodes. One possible path through the graph is shown in red.

classification for each electrode. An example path is shown in red in Fig. 2. This example path implies a ST cavity classification for electrodes 1 and N and a BM classification for electrodes 2 and 3 because it passes through the top (ST) row in the columns corresponding to electrodes 1 and N, and through the bottom (BM) row for electrodes, 2 and 3. To use this graph to find an accurate cavity classification, we need to define appropriate cost values for the set of edges E. Then we can use standard graph searching methods, such as Dijkstra's algorithm [10], to find the path with the globally minimum cost.

We define two types of cost for our edge cost function, "class cost" and "transition cost," which are the electrode classification cost, and the class transition cost. Let $C(V_j)$ and $P(V_j)$ represent the cavity classification and the electrode associated with node V_j, respectively. Then, the class cost for an edge $E_{i,j}$ connecting node V_i to V_j represents the cost for assigning the electrode represented by V_j, $P(V_j)$, to the cavity classification associated with V_j, $C(V_j)$, and is defined by

$$\text{class}(V_j) = \left\{ \begin{array}{cc} D_{\text{ST}}(P(V_j)) - d_{\min} + \alpha & C(V_j) = \text{ST} \\ D_{\text{SV}}(P(V_j)) - d_{\min} + \alpha & C(V_j) = \text{SV} \\ \left| D_{\text{ST}}(P(V_j)) - D_{\text{SV}}(P(V_j)) \right| & C(V_j) = \text{BM} \end{array} \right\}, \tag{1}$$

where

$$d_{\min} = \min\left(D_{\text{ST}}(P(V_j)),\ D_{\text{SV}}(P(V_j))\right), \tag{2}$$

D_{ST} and D_{SV} are signed-distance map representations of the scala tympani and scala vestibuli computed using fast marching techniques [11] with negative distances in the structure foreground and positive distances in the background, $D(P)$ is the value of the signed distance map at electrode P, and α is a parameter tuned as described in the following section that controls the width of the region between the scala tympani and vestibuli that is considered to be the basilar membrane region. If the electrode $P(V_j)$ falls 0.5α mm within the border of the scala vestibuli, then $D_{\text{SV}}(P(V_j)) = -0.5\alpha$, $D_{\text{ST}}(P(V_j)) \geq 0.5\alpha$, $d_{\min} = -0.5\alpha$, and $\left| D_{\text{ST}}(P(V_j)) - D_{\text{SV}}(P(V_j)) \right| \geq \alpha$. In this case, the classification cost for assigning $P(V_j)$ to SV, BM, or ST, would be α, $\geq \alpha$, and $\geq 2\alpha$. Thus, the highest cost is assigned to ST classification. If the electrode sits farther than 0.5α mm from the scala tympani, the second highest cost would be to BM classification.

Otherwise SV and BM are assigned equal cost because the electrode falls on the border between the SV and the α mm wide BM region we have defined between the ST and SV.

The transition cost for edge $E_{i,j}$ represents the cost for transitioning classifications from $C(V_i)$ to $C(V_j)$ and is defined by

$$\text{transition}(V_i, V_j) = \left\{ \begin{array}{ll} \beta & C(V_i) \neq C(V_j) \\ 0 & C(V_i) = C(V_j) \end{array} \right\}, \tag{3}$$

where β is a constant to punish class inconsistency among neighboring electrodes and is tuned as described in the following section. The overall cost function is defined as

$$cost(E_{i,j}) = \left\{ \begin{array}{cc} \text{class}(V_j) + \text{transition}(V_i, V_j) & C(V_i) \neq C(V_j) \\ \text{class}(V_j) & C(V_i) = C(V_j) \text{ or } C(V_i) = \text{seed} \\ 0 & C(V_j) = \text{endnode} \end{array} \right\},$$

where these three types of edges are shown as green, black, and gray edges in the graph in Fig. 2.

Finally, it is also common for some electrodes to be outside the cochlea when the surgeon stops inserting the array prior to those electrodes entering the cochlea. To detect which electrodes are outside of the cochlea, we find the first electrode in the array that falls within the foreground of the ST or SV segmentations and classify all previous electrodes as falling outside of the cochlea.

Parameter Selection and Validation. We trained parameters and evaluated our approach simultaneously using a leave-one-out validation study. In this process, our two parameters α and β were tuned using 33 of the 34 datasets and then tested on the left-out dataset. This process was repeated so that the method was tested on each of the 34 datasets while leaving that testing set out of the training process. To train our parameters, first, heuristic tuning was done on one case. We started with values 0.3 and 0.15 for α and β and found 0.2 and 0.3 to lead to better results. Then, these values were used as initial values when performing the parameter optimization in all cases. For each testing case, these parameters were iteratively optimized on the training dataset until converging to a local classification error minimum. Classification errors were defined as the sum of incorrect cavity classifications relative to the ground truth classification across all training sets. The ground truth cavity classification for each electrode was defined by visual inspection of the raw high resolution μCT images, where cavity borders are visible, in an interactive viewer with three 2D orthogonal planar views without the benefit of the automated image processing data. Within each iteration of the parameter search, each parameter was independently varied from its initial value in the range [−0.125, 0.125] in steps of 0.025. A new value for the parameter was selected as the value that resulted in minimum overall error. Because the cost function is discrete, it often can result in multiple equal minima. When separate multiple minima were present, preference was given to the minimum closest to the initial value. When three or more adjacent values resulted in identical minimal error, preference was given to values that were not adjacent to non-minimal values in order to choose values that corresponded to locations within, rather than on the edge of, the minimum region.

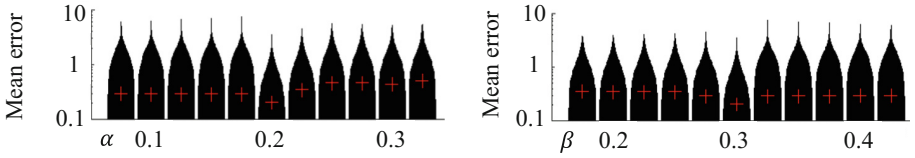

Fig. 3. Violin plots of classification errors made in the entire dataset when sweeping parameters α (left) and β (right) around their final values.

Table 1. Confusion matrices and classification results of the leave-one-out experiment, when using the final selected parameters on the entire dataset, and when not using the proposed graph search method.

		Results with leave-one-out				Results with final parameters				Results without graph search			
		OC	ST	SV	BM	OC	ST	SV	BM	OC	ST	SV	BM
Ground Truth	OC	32	2	0	0	32	2	0	0	32	0	0	2
	ST	1	506	2	0	1	506	2	0	1	458	2	48
	SV	0	0	30	0	0	0	30	0	0	0	27	3
	BM	0	5	0	0	0	2	0	3	0	2	0	3
Sensitivity (%)		94.1	99.4	100.0	0.0	94.1	99.4	100.0	60.0	94.1	90.0	90.0	60.0
Specificity (%)		99.8	89.9	99.6	100.0	99.8	94.2	99.6	100.0	99.8	97.1	99.6	90.8

3 Results

A local optimum of both parameters was successfully obtained for every leave-one-out parameter search. In 1 of 34 test cases (case #12), the parameter search selected α and β as 0.175 and 0.3. In the remaining 33 of 34 test cases, the parameter search converged to values of 0.2 and 0.3. Thus, these values appear to correspond to a stable optimum and we select them as the final parameter values. Violin plots of the number of classification errors for each dataset when sweeping these parameters around their final parameter values is shown in Fig. 3. The mean of the number of errors for each case is shown as a red cross for each parameter value. As can be seen in the figure, values of 0.2 and 0.3 for α and β correspond to a clear local minimum of classification error.

Overall classification results are shown in Table 1. When using the trained parameters found in the leave-one-out tests, we achieve overall classification accuracy of 98%, and excellent specificity and sensitivity for the ST, SV, and Out of Cochlea (OC) classifications. However, our method achieves 0% sensitivity for the BM class. This is because the BM class is highly underrepresented in our dataset, with all of the only 5 BM electrodes belonging to case #12. Thus, when leave-one-out testing on case #12, there were zero BM electrodes in the training set, and it is unsurprising that the resulting leave-one-out trained α was selected low enough to lead to 0% BM sensitivity. When using the final selected parameters on the whole dataset, overall accuracy is 99% and BM sensitivity is 60%, which is still low but unsurprising considering the BM class is only represented by 5 of 578 electrodes in our dataset.

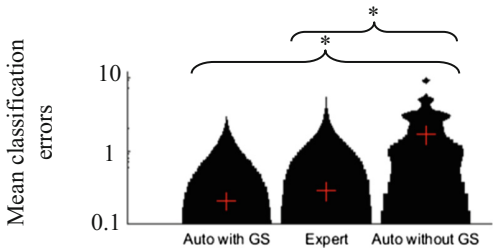

Fig. 4. Final results shown as violin plots of the proposed automatic method with graph search (GS), expert determination of the cavity positioning, and automatic cavity localization without the graph search method we propose.

We also compared the leave-one-out classification results to expert classification and automatic classification using the image processing data directly without the benefit of the robustness-boosting graph search method we propose. These results are shown as violin plots in Fig. 4 and confusion matrix in Table 1. Expert classification of cavity position for each electrode was done by inspection of the CT images and image processing data (electrode localization and anatomy segmentation) in an interactive viewer with 3D views and three 2D orthogonal planar views without the benefit of the high resolution μCT. The expert classification results are found to have a slightly higher mean error than our proposed method, although this difference was not found to be statistically significant using a paired t-test. Both the proposed method and expert classification perform statistically significantly better (p < 1e-4) than automatic classification without the graph search method proposed in this work.

4 Conclusions

In this work, we have proposed a novel and fully automatic method for identification of the cavity position of intracochlear electrodes. Our experiments show that our method has high classification accuracy. Compared to expert cavity identification, our method produces comparable results. Compared to non-robust cavity identification techniques, our method produces significantly more accurate results. Our approach is also fast, requiring less than a second of processing time after a 5 min procedure is used to automatically localize the anatomical structures and electrode array.

While overall classification accuracy is high, our method results in poor sensitivity for BM classification because this class is inadequately represented in our dataset. In future work, we will expand our ground truth dataset to attempt to obtain more examples of electrodes located in the BM region to explore whether our method can achieve acceptable BM classification sensitivity when using a more balanced training dataset. We also plan to apply our method to large numbers of clinical datasets to facilitate studying how the location of individual electrodes correlates with outcomes with the goal of developing technologies that can improve hearing outcomes with CIs.

Acknowledgements. This work was supported in part by grants R01DC014037 and R01DC014462 from the NIDCD. The content is solely the responsibility of the authors and does not necessarily represent the official views of this institute.

References

1. "Cochlear Implants," National Institute on Deafness and Other Communication Disorders, No. 11–4798 (2011)
2. Verbist, B.M., Frijns, J.H.M., Geleijns, J., van Buchem, M.A.: Multisection CT as a valuable tool in the postoperative assessment of cochlear implant patients. Am J Neuroradiol **26**, 424–429 (2005)
3. Aschendorff, A., et al.: Quality control after cochlear implant surgery by means of rotational tomography. Otol. Neurotol. **26**, 34–37 (2005)
4. Skinner, M.W., et al.: In vivo estimates of the position of advanced bionics electrode arrays in the human cochlea. Ann. Otol. Rhinol. Laryngol. Suppl. **197**, 2–24 (2007)
5. Wanna, G.B., et al.: Assessment of electrode placement and audiologic outcomes in bilateral cochlear implantation. Otol. Neurotol. **32**, 428–432 (2011)
6. Wanna, G.B., et al.: Impact of electrode design and surgical approach on scalar location and cochlear implant outcomes. Laryngoscope **124**(S6), S1–S7 (2014)
7. Noble, J.H., Dawant, B.M.: Automatic graph-based localization of cochlear implant electrodes in CT. In: Navab, N., Hornegger, J., Wells, W.M., Frangi, A.F. (eds.) MICCAI 2015. LNCS, vol. 9350, pp. 152–159. Springer, Cham (2015). https://doi.org/10.1007/978-3-319-24571-3_19
8. Zhao, Y., Dawant, B.M., Labadie, R.F., Noble, J.H.: Automatic localization of cochlear implant electrodes in CT. In: Golland, P., Hata, N., Barillot, C., Hornegger, J., Howe, R. (eds.) MICCAI 2014. LNCS, vol. 8673, pp. 331–338. Springer, Cham (2014). https://doi.org/10.1007/978-3-319-10404-1_42
9. Noble, J.H., Labadie, R.F., Majdani, O., Dawant, B.M.: Automatic segmentation of intracochlear anatomy in conventional CT. IEEE Trans. on Biomedical. Eng. **58**(9), 2625–2632 (2011)
10. Dijkstra, E.W.: A note on two problems in connexion with graphs. Numer. Math. **1**, 269–271 (1959)
11. Sethian, J.A.: Level Set Methods and Fast Marching Methods, 2nd edn. Cambridge University Press, Cambridge (1999)